A CFD–PBM Coupled Model for Gas–Liquid Flows

Tiefeng Wang, Jinfu Wang, and Yong Jin
Dept. of Chemical Engineering, Tsinghua University, Beijing 100084, China

DOI 10.1002/aic.10611
Published online September 13, 2005 in Wiley InterScience (www.interscience.wiley.com).

A computational fluid dynamics–population balance model (CFD-PBM) coupled model was developed that combines the advantages of CFD to calculate the entire flow field and of the PBM to calculate the local bubble size distribution. Bubble coalescence and breakup were taken into account to determine the evolution of the bubble size. Different bubble breakup and coalescence models were compared. An algorithm was proposed for computing the parameters based on the bubble size distribution, including the drag force, transverse lift force, wall lubrication force, turbulent dispersion force, and bubble-induced turbulence. With the bubble breakup and coalescence models and the interphase force formulations in this work, the CFD-PBM coupled model can give a unified description for both the homogeneous and the heterogeneous regimes. Good agreement was obtained with the experimental results for the gas holdup, liquid velocity, and bubble size distribution. © 2005 American Institute of Chemical Engineers *AIChE J,* 52: 125–140, 2006
Keywords: computational fluid dynamics (CFD), population balance model (PBM), bubble size distribution, coalescence, breakup

Introduction

Gas–liquid reactors, such as bubble columns and airlift loop reactors, are widely used in chemical and biochemical processes because of their excellent mass- and heat-transfer characteristics and simple construction. However, their fundamental hydrodynamic behaviors, which are essential for reactor scale-up and design, are still not fully understood. To develop design tools for engineering purposes, much research has been carried out in the area of computational fluid dynamics (CFD) modeling and simulation of gas–liquid flows. Two approaches are primarily used: the *Euler–Lagrange* (Delnoij et al., 1997; Sokolichin et al., 1997) and the *Euler–Euler* approach (Drew, 1983; Ishii, 1975; Krishna et al., 1999; Lahey and Drew, 1992; Lehr et al., 2002). The Euler–Lagrange approach has the advantage of a clear physical description but the disadvantage of high computational cost and the difficulties of considering the forces on the deformable bubbles and bubble breakup and coalescence. The Euler–Euler approach has the advantage that the model equations for each phase have the same form and the simulations need much less computations. Therefore the Euler–Euler approach was used in this work.

In most CFD simulations of dispersed gas–liquid flow, the local bubble size distribution is not used and a constant bubble size is used instead. This simplification limits such models to the homogeneous regime. In fact, it is very important to consider in detail the local bubble behavior for the following reasons:

(1) The bubble behavior has a significant influence on the flow regime transition because the major phenomenon causing the transition from the homogeneous to the heterogeneous regime is the occurrence of large bubbles.

(2) The bubble size has a wide distribution in the heterogeneous regime, which is the usual case for an industrial gas–liquid reactor.

(3) The complexity of bubble dynamics makes the radial profiles of the gas holdup and bubble rise velocity difficult to predict for a wide variety of conditions (Jakobsen et al., 1997; Joshi, 2001). This is because the radial profile of the gas holdup is determined by the lateral forces, such as the transverse lift force, turbulent dispersion force, and wall lubrication force, and these lateral forces depend on the bubble size (Lucas et al., 2001; Tomiyama et al., 1999). However, the lateral forces are ignored or simplified in most CFD simulations reported in the

Correspondence concerning this article should be addressed to J.-F. Wang at wangjf@flotu.org.

literature (Hua and Wang, 2000; Pan et al., 1999; Pfleger and Becker, 2001).

(4) Bubble breakup and coalescence have a significant influence on the interphase mass transfer.

Because of the importance of the bubble behavior, great efforts have been made in recent years to couple the PBM into the computational fluid dynamics. This concept was implemented as the so-called *multiple-size-group* (MUSIG) model in the commercial CFD package, CFX. However. the bubble breakup and coalescence models used in CFX cannot give proper predictions in wide operating conditions. Several authors have made attempts to couple their own bubble breakup and coalescence models into the CFD framework. Chen et al. (2005) used the population balance model with different bubble breakup and coalescence closures, and concluded that the choice of bubble breakup and coalescence closure does not have a significant influence on the simulated results as long as the magnitude of breakup is increased tenfold. This conclusion is not consistent with the results of Wang et al. (2005), where four typical bubble coalescence and breakup modes (Lehr et al., 2002; Luo and Svendsen, 1996a,b; Prince and Blanch, 1990; Wang et al., 2003, 2005) were compared. The results show that the bubble size distributions are quite different when different bubble coalescence and breakup models are used. The bubble breakup and coalescence models are very important for proper prediction of the bubble size distributions in different flow regimes.

The two-fluid model with the assumption of constant bubble diameter can give reasonable predictions for the homogeneous regime because the bubble size distribution in such a condition is narrow and the bubble interaction is relatively weak. The most important issue of the computational fluid dynamics–population balance model (CFD-PBM) coupled model is therefore its ability to predict the hydrodynamics in the heterogeneous regime where bimodal bubble size distributions are observed, especially in high superficial gas velocities. However, most reported results by the CFD-PBM coupled model are either only for the homogeneous regime (Colella et al., 1999; Sha et al., 2004) or for both the homogeneous and the heterogeneous regimes but do not successfully predict bimodal bubble size distribution in the heterogeneous regime (Chen et al., 2005; Olmos et al., 2001). One exception is found in the results of Lehr et al. (2002), where the bimodal bubble size distributions are obtained. Lehr et al. (2002) reported the three-dimensional (3-D) transient simulation results, in which the population balance was simplified to a balance equation for the average bubble volume. The gas phase was modeled as small and large bubble phases, and the small and large bubble fractions were calculated by the simplified balance equation. The bubble size was calculated with the assumption that the dimensionless number density distributions of the small and large bubble fractions are approximated by a lognormal distribution and an exponential distribution, respectively.

Such simplification remarkably reduces the computational demands and makes the 3-D transient simulations feasible. However, this simplification approach particularly depends on their bubble breakup and coalescence models and may be infeasible for other models. The interphase drag force in their model was calculated with the Sauter mean diameter but not directly based on the bubble size distribution. Further, they neglected the wake effect of large bubbles on the interphase drag force, which is important in the heterogeneous regime (Krishna et al., 1999). The lateral forces were also neglected in their work. Experimental study and numerical simulations have proved that lateral forces are important for the formation of different radial profiles of the gas holdup (Liu and Bankoff, 1993; Lucas et al., 2001; Tomiyama et al., 1999; Wang et al., 2004b). Two types of radial profiles of the gas holdup were observed: wall-peaking and core-peaking profiles. For large bubbles the transverse lift force acts to the central region and the gas holdup has a core-peaking profile, whereas for small bubbles the transverse lift force acts to the wall and the gas holdup has a wall-peaking profile. Therefore, it is necessary to consider the lateral forces for correct prediction of different radial profiles of the gas holdup. All the reported simulations that neglect the lateral forces predict a flat or core-peaking radial profile of the gas holdup. These models cannot predict the wall-peaking radial profile of the gas holdup in a system with small bubbles.

In this work, a full population balance model with detailed bubble breakup and coalescence models is coupled in the CFD framework. Different bubble breakup and coalescence models are compared. An algorithm is proposed to calculate the interphase forces and turbulence modification based on the bubble size distribution. The ability of the CFD-PBM coupled model to predict the hydrodynamics both in the homogeneous and heterogeneous regime is discussed in detail. The advantages of the CFD-PBM coupled model developed in this work are such that it: (1) has both the ability of CFD to calculate the entire flow field and the ability of the PBM to calculate the local bubble size distribution; (2) combines the PBM into the CFD framework so that bubble breakup and coalescence can be taken into account, and the CFD-PBM coupled model can describe the bubble size distribution in different flow regimes; (3) takes into account the influence of the bubble size on the interphase interaction so that the CFD-PBM coupled model has the ability to predict the flow behavior in different flow regimes; and (4) predicts the local bubble size distribution and gas holdup from which the local gas–liquid interfacial area can be determined.

With the consideration that two-dimensional (2-D) computations are much faster than 3-D simulations, and in many cases only time-averaged results are of interest for purpose of reactor simulation and design, we used the 2-D steady-state approach in this work and focused on the coupling between the population balance model and the computational fluid dynamics. It should be pointed out that, on the one hand, the real observed bubble column flows are highly transient and turbulent with vortical bubble swarms, and never reach a steady state. On the other hand, time averaging produces reproducible stationary patterns, and the experiments had shown repeatedly (Degaleesan et al., 2001; Hills, 1974; Ohnuki and Akimoto, 2000; Svendsen et al., 1992) that, in the time-averaged sense, there is a stationary axisymmetric flow pattern in a cylindrical bubble column. Therefore, although 2-D axisymmetric steady-state simulations cannot predict the highly transient flow fields, they are reasonable for the time-averaged flow fields in bubble columns. Such models have been used by several authors (Hua and Wang, 2000; Jakobsen et al., 1997; Thakre and Joshi, 1999) and achieve reasonable results compared with the experimental measurements.

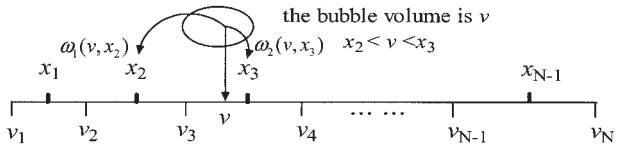

Figure 1. Bubble size division and bubble redistribution.

PBM Equations

The population balance model, first formulated for chemical engineering purposes by Hulburt and Katz (1964), has drawn much attention from both academic and industrial researchers because it can describe the size distribution of the dispersed phase in a wide variety of particulate processes (Colella et al., 1999; Kostoglou and Karabelas, 1998; Kronberger et al., 1995; Lehr and Mewes, 2001; Millies and Mewes, 1999; Olmos et al., 2001; Pohorecki et al., 2001; Ramkrishna and Mahoney, 2002; Venneker et al., 2002). The PBM is a statistical equation that describes the dispersed phase in a multiphase flow. The PBM equation for the gas–liquid bubbly flow can be expressed as follows (Ramkrishna, 2000)

$$\underbrace{\frac{\partial n(v,t)}{\partial t}}_{I} + \underbrace{\nabla\cdot[\mathbf{u}_b n(v,t)]}_{II} = \underbrace{\frac{1}{2}\int_0^v n(v-v',t)n(v',t)c(v-v',v')dv'}_{III} - \underbrace{\int_0^\infty n(v,t)n(v',t)c(v,v')dv'}_{IV} + \underbrace{\int_v^\infty \beta(v,v')b(v')n(v',t)dv'}_{V} - \underbrace{b(v)n(v,t)}_{VI} \quad (1)$$

where the bracketed terms describe (*I*) time variation, (*II*) convection, (*III*) source ascribed to coalescence, (*IV*) sink ascribed to coalescence, (*V*) source ascribed to breakup, and (*VI*) sink ascribed to breakup. Equation 1 is an integrodifferential equation, and different approaches have been proposed in the literature to solve this equation. The discrete method developed by Kumar and Ramkrishna (1996) was used in this work. In this method, the bubble size is divided into a number of intervals and each interval is represented by a pivot size x_i, as shown in Figure 1. Equation 1 was integrated over each size interval, say $[v_i, v_{i+1}]$, resulting in the following expressions

$$\underbrace{\frac{\partial N_i(t)}{\partial t}}_{I'} + \underbrace{\nabla\cdot[\mathbf{u}_b N_i(t)]}_{II'} = \underbrace{\frac{1}{2}\int_{v_i}^{v_{i+1}} dv \int_0^v n(v-v',t)n(v',t)c(v-v',v')dv'}_{III'} - \underbrace{\int_{v_i}^{v_{i+1}} n(v,t)dv \int_0^\infty n(v',t)c(v,v')dv'}_{IV'} + \underbrace{\int_{v_i}^{v_{i+1}} dv \int_v^\infty \beta(v,v')b(v')n(v',t)dv'}_{V'} - \underbrace{\int_{v_i}^{v_{i+1}} b(v)n(v,t)dv}_{VI'} \quad (2)$$

where N_i is the number of bubbles of volume between v_i and v_{i+1}.

An accurate determination of the terms on the right-hand side (rhs) of Eq. 2 requires a knowledge of $n(v, t)$, that is, the set of equations is not closed. A closed set of equations can be obtained by representing the rhs of Eq. 2 in terms of N_i (Kumar and Ramkrishna, 1996). The population in a representative volume x_i gets a fractional bubble for every bubble born in the size range (x_i, x_{i+1}) or (x_{i-1}, x_i). For bubbles born in the range (x_i, x_{i+1}), $\omega_1(v, x_i)$ bubbles are assigned to x_i, and for those born in the range (x_{i-1}, x_i), $\omega_2(v, x_i)$ bubbles are assigned, as shown in Figure 1. The values of $\omega_1(v, x_i)$ and $\omega_2(v, x_i)$ are given by

$$\omega_1(v, x_i)x_i + \omega_2(v, x_{i+1})x_{i+1} = v \quad (3)$$

$$\omega_1(v, x_i) + \omega_2(v, x_{i+1}) = 1 \quad (4)$$

Taking the source term ascribed to coalescence as an example, term *III′* in Eq. 2 is modified to

$$\frac{1}{2}\int_{x_i}^{x_{i+1}} \omega_1(v, x_i)dv \int_0^v n(v-v', t)n(v', t)c(v-v', v')dv' + \frac{1}{2}\int_{x_{i-1}}^{x_i} \omega_2(v, x_i)dv \int_0^v n(v-v', t)n(v', t) \times c(v-v', v')dv' \quad (5)$$

Note that

$$n(v, t) = \sum_{k=1}^{M} N_k(t)\delta(v - x_k) \quad (6)$$

Substituting Eq. 6 into Eq. 5 yields

$$\sum_{\substack{j,k \\ x_{i-1}\le(x_j+x_k)\le x_{i+1}}}^{j\ge k} \left(1 - \frac{1}{2}\delta_{j,k}\right)\eta_{i,jk}c_{j,k}N_j(t)N_k(t) \quad (7)$$

where

$$\eta_{i,jk} = \begin{cases} (x_{i+1} - v)/(x_{i+1} - x_i), & x_i < v \le x_{i+1} \\ (v - x_{i-1})/(x_i - x_{i-1}), & x_{i-1} < v \le x_i \end{cases} \qquad v = v_j + v_k \quad (8)$$

Other terms in Eq. 2 are reconstructed similarly and the final discrete PBM is expressed as

$$\underbrace{\frac{dN_i(t)}{dt}}_{I'} + \underbrace{\nabla \cdot [\mathbf{u}_b N_i(t)]}_{II'} = \underbrace{\sum_{\substack{j,k \\ x_{i-1} \le (x_j + x_k) \le x_{i+1}}}^{j \ge k} \left(1 - \frac{1}{2}\delta_{j,k}\right) \eta_{i,jk} c_{j,k} N_j(t) N_k(t)}_{III''} - \underbrace{N_i(t) \sum_{k=1}^{M} c_{i,k} N_k(t)}_{IV''} + \underbrace{\sum_{k=i}^{M} \zeta_{i,k} b_k N_k(t)}_{V''} - \underbrace{b_i N_i(t)}_{VI''} \quad (9)$$

$$\zeta_{i,k} = \int_{x_i}^{x_{i+1}} \frac{x_{i+1} - v}{x_{i+1} - x_i} \beta(v, x_k) dv + \int_{x_{i-1}}^{x_i} \frac{v - x_{i-1}}{x_i - x_{i-1}} \beta(v, x_k) dv \quad (10)$$

To solve Eq. 9, the bubble coalescence kernel function $c(v, v')$, bubble breakup kernel function $b(v)$, and daughter bubble size distribution $\beta(v, v')$ are needed.

Coalescence kernel functions

Three main mechanisms of bubble coalescence exist in a gas–liquid system: coalescence resulting from turbulent eddies, coalescence resulting from different rise velocities, and coalescence resulting from bubble wake entrainment (Fu and Ishii, 2002; Prince and Blanch, 1990). The total coalescence rate is assumed to be the linear sum of the rates arising from these different mechanisms. In most works reported in the literature, only the coalescence resulting from turbulent eddies was considered. This simplification may be reasonable at medium superficial gas velocities because coalescence arising from turbulent eddies is the main mechanism under such conditions. However, at high superficial gas velocities, bubble coalescence resulting from wake entrainment is important for the formation of large bubbles. Furthermore, bubble coalescence resulting from different bubble rise velocities cannot be ignored when the bubble rise velocity is sensitive to the bubble size. For the correct prediction of the bubble size distributions in both homogeneous and heterogeneous regimes, all three coalescence mechanisms above were considered in this work. The coalescence rate of bubbles of size d_i and d_j can be expressed by

$$c(d_i, d_j) = \varpi(d_i, d_j) P(d_i, d_j) \quad (11)$$

where ϖ and P are the collision frequency and the coalescence efficiency, respectively.

Coalescence Resulting from Turbulent Eddies

- *Collision frequency*

Bubble collisions resulting from turbulent eddies were calculated by analogy with gas kinetic theory (Prince and Blanch, 1990)

$$\varpi_c(d_i, d_j) = \frac{\pi}{4} (d_i + d_j)^2 \bar{u}_{ij} \quad (12)$$

where the relative turbulent velocity $\bar{u}_{ij}$ between bubbles of size d_i and d_j is

$$\bar{u}_{ij} = (\bar{u}_i^2 + \bar{u}_j^2)^{1/2} \quad (13)$$

The mean turbulent velocity of a bubble of size d_i is considered to be the same as the mean turbulent velocity of an eddy of the same size, which can be calculated as (Levich, 1962)

$$\bar{u}_\lambda = \sqrt{2}(\varepsilon\lambda)^{1/3} \quad (14)$$

Substituting Eq. 14 into Eq. 13 yields

$$\bar{u}_{ij} = \sqrt{2}\, \varepsilon^{1/3} (d_i^{2/3} + d_j^{2/3})^{1/2} \quad (15)$$

In Eq. 12, two effects were not taken into account: the ratio of the bubble turbulent path to the distance between bubbles and the reduction of the free space for bubble movement arising from the volume occupied by the bubbles. When the distance between bubbles is larger than the bubble turbulent path, the actual bubble collision frequency is less than the value calculated by Eq. 12. The reduction of the free space for bubble movement causes an increase in the bubble collision frequency. The final equation for bubble collision frequency including these two effects is expressed as

$$\varpi_c(d_i, d_j) = \frac{\pi}{4} \frac{\alpha_{g,\max}}{\alpha_{g,\max} - \alpha_g} \Gamma_{ij} \sqrt{2}\, \varepsilon^{1/3} (d_i + d_j)^2 (d_i^{2/3} + d_j^{2/3})^{1/2} \quad (16)$$

where $\alpha_{g,\max}$, the maximum gas holdup, is set to be 0.8 in this work. Γ_{ij} depends on the ratio between the bubble turbulent path length and the distance between bubbles, and was correlated as

$$\Gamma_{ij} = \exp[-(l_{bt,ij}/h_{b,ij})^{6.0}] \quad (17)$$

where $l_{bt,ij}$ is the mean relative turbulent path length of bubbles of size d_i and d_j

$$l_{bt,ij} = (l_{bt,i}^2 + l_{bt,j}^2)^{1/2} \quad (18)$$

The bubble turbulent path length l_{bt} is assumed to be equal to the distance that a turbulent eddy of size d_b moves during its lifetime τ_e

$$l_{bt} = \bar{u}_{bt}\tau_e = \sqrt{2}(\varepsilon d_b)^{1/3}(r_b^2/\varepsilon)^{1/3} \approx 0.89 d_b \quad (19)$$

$h_{b,ij}$ in Eq. 17 is related to the mean distance between bubbles of size d_i and d_j, and was calculated by

$$h_{b,ij} = k(n_i + n_j)^{-1/3} \quad (20)$$

where $n_i = N_i/\Delta d_i$, and Δd_i is the diameter increment in the ith bubble size region. k was set to be 6.3 according to the measured bubble size distribution.

- *Coalescence efficiency*

Up to now, models for bubble coalescence efficiency are mainly based on a phenomenological analysis. According to

bubble coalescence theory, coalescence will occur during a collision of two bubbles provided that the contact time exceeds the coalescence time required for drainage of the liquid film between them to a critical rupture thickness (Chesters, 1991). The ratio between the contact time τ and the coalescence time t can thus provide a first indication of whether coalescence will occur. The following function has been used by Lee et al. (1987), Prince and Blanch (1990), and Chesters (1991)

$$P_c(d_i, d_j) = \exp\left(-\frac{t_{ij}}{\tau_{ij}}\right) \tag{21}$$

Chesters (1991) estimated the coalescence time, based on a drainage model for full interfacial mobility and inertial control condition, as

$$t_{ij} = 0.5\,\frac{\rho_l \bar{u}_{ij} d_i^2}{(1+\xi_{ij})2\sigma} \tag{22}$$

where $\xi_{ij} = d_i/d_j$.

Luo and Svendsen (1996a) proposed a model for the bubble interaction time by energy conservation analysis. Their expression reads

$$\tau_{ij} = (1+\xi_{ij})\sqrt{\frac{(\rho_g/\rho_l)+C_{VM}}{3(1+\xi_{ij}^2)(1+\xi_{ij}^3)}\,\frac{\rho_l d_i^3}{\sigma}} \tag{23}$$

Substituting Eqs. 22 and 23 into Eq. 21 yields

$$P_c(d_i, d_j) = \exp\left\{-\frac{[0.75(1+\xi_{ij}^2)(1+\xi_{ij}^3)]^{1/2}}{(\rho_g/\rho_l + C_{VM})(1+\xi_{ij})^3}\,\mathrm{We}_{ij}^{1/2}\right\} \tag{24}$$

Coalescence Resulting from Wake Entrainment. A large bubble with a sphere-cap shape has a strong wake region. Other bubbles will be accelerated when entering such bubble wake regions, which results in bubble collision and coalescence.

- *Collision frequency*

The bubble collision frequency ascribed to wake entrainment is related to the bubble number and the bubble rise velocity in the effective wake region of leading large bubbles. If the mean time of the entrained bubbles colliding with the leading large bubble is ΔT, the collision frequency can be calculated as

$$\varpi_w(d_i, d_j) = k_1 N_{wi,j}/(N_j \Delta T) \tag{25}$$

where $N_{wi,j}$ is the number of bubbles of size d_j in the wake region of a leading large bubble of size d_i, and is determined by

$$N_{wi,j} = V_{wi} N_j = \frac{\pi}{4} d_i^2 \left(L_w - \frac{d_i}{2}\right) N_j \tag{26}$$

where V_{wi} is the volume of the effective wake region of a leading bubble of size d_i. Combining Eqs. 25 and 26 yields

$$\varpi_w(d_i, d_j) = \frac{\pi}{4} k_1 k_2 d_i^2 \bar{u}_{wi,j} \tag{27}$$

where $\bar{u}_{wi,j}$ is the bubble rise velocity relative to the leading bubble. Schlichting (1979) and Bilicki and Kestin (1987) gave the following correlation

$$\bar{u}_{wi,j} = \frac{\kappa \bar{u}_{slip,i}}{L_w/d_i - 1/2}\left[\left(\frac{L_w}{d_i/2}\right)^{1/3} - 1\right] \tag{28}$$

where L_w is the effective length of the bubble wake, $\bar{u}_{slip,i}$ is the rise velocity of the leading bubble, and κ is a model parameter.

Combining Eqs. 27 and 28 yields

$$\varpi_w(d_i, d_j) = \frac{\pi}{4}\Theta k_1 k_2 \frac{\gamma}{L_w/d_i - 1/2}\left[\left(\frac{L_w}{d_i/2}\right)^{1/3} - 1\right] \times d_i^2 \bar{u}_{slip,i} = K\Theta d_i^2 \bar{u}_{slip,i} \tag{29}$$

The parameter K in Eq. 29 was set to be 12.0 for reasonable prediction of the bubble size distribution in both the homogeneous and the heterogeneous regimes. $\bar{u}_{slip,i}$ was calculated by

$$\bar{u}_{slip,i} = 0.71\sqrt{g d_i} \tag{30}$$

The parameter Θ in Eq. 29, which was introduced with the consideration that only bubbles larger than d_c has a wake region effective for bubble coalescence, is calculated as

$$\Theta = \begin{cases} \left(d_j - \frac{d_c}{2}\right)^6 \Big/ \left[\left(d_j - \frac{d_c}{2}\right)^6 + \left(\frac{d_c}{2}\right)^6\right] & d_j \geq d_c/2 \\ 0 & \text{else} \end{cases} \tag{31}$$

The value of d_c can be estimated as follows (Ishii and Zuber, 1979)

$$d_c = 4\sqrt{\frac{\sigma}{g\Delta\rho}} \tag{32}$$

- *Coalescence efficiency*

The coalescence probability was calculated by the correlation of Hibiki and Ishii (2000)

$$P_w(d_i, d_j) = \exp\left[-0.46\,\frac{\rho_l^{1/2}\varepsilon^{1/3}}{\sigma^{1/2}}\left(\frac{d_i d_j}{d_i + d_j}\right)^{5/6}\right] \tag{33}$$

Coalescence Resulting from Different Rise Velocities. The model for bubble coalescence resulting from different rise velocities is similar to that resulting from turbulent eddies, except that the characteristic velocity $(\bar{u}_i^2 + \bar{u}_j^2)^{1/2}$ in Eq. 13 is replaced by $|u_{bi} - u_{bj}|$, where u_{bi} and u_{bj} are the rise velocities of bubbles of size d_i and d_j, respectively. Because the bubbles rise vertically, the modification by Eq. 17 is unnecessary. The bubble coalescence efficiency was set to be 0.5 by fitting the measured bubble size distribution at low superficial gas velocities.

Breakup kernel functions

Two main mechanisms for bubble breakup were considered: breakup resulting from eddy collision and breakup resulting from the instability of large bubbles. The total breakup rate was calculated by summing the rates arising from these two mechanisms. In low to medium gas holdups, the former is the main mechanism, whereas the latter becomes larger with an increase in the gas holdup.

Breakup Resulting from Eddy Collision. Wang et al. (2003) proposed a breakup kernel function based on an eddy–bubble interaction mechanism. This model accounted for both the energy constraint and the capillary constraint, and gave more reasonable results than the model of Luo and Svendsen (1996b). The model is briefly described here and details can be found in our previous work (Wang et al., 2003). The breakup kernel function can be calculated by

$$b(f_v|d) = \int_{\lambda_{\min}}^{d} P_b(f_v|d, \lambda)\varpi_\lambda(d)d\lambda \tag{34}$$

where $P_b(f_v \mid d, \lambda)$ is the probability density that a bubble of size d or volume v breaks into two bubbles, one with volume vf_v and the other with $v(1 - f_v)$, when the bubble is hit by a turbulent eddy of size λ. $\varpi_\lambda(d)$ is the collision frequency of eddies of size between λ and $\lambda + d\lambda$ with bubbles of size d, which is determined in analogy to gas kinetic theory. The final formula reads (Luo and Svendsen, 1996b; Prince and Blanch., 1990)

$$\varpi_\lambda(d) = 0.923(1 - \alpha_g)n\varepsilon^{1/3}\frac{(\lambda + d)^2}{\lambda^{11/3}} \tag{35}$$

When a bubble of size d is hit by an eddy of size λ and kinetic energy $e(\lambda)$, the daughter bubble size is limited by a minimum as a result of capillary pressure and by a maximum arising from the increase in the surface energy. When a bubble breakup occurs, the dynamic pressure attributed to the eddy turbulence should satisfy the following equation

$$\frac{\rho_c u_\lambda^2}{2} \geq \frac{\sigma}{d_1} \tag{36}$$

that is,

$$d_1 \geq \frac{\sigma V_\lambda}{e(\lambda)} \qquad f_{v,\min} = \left[\frac{\pi\lambda^3\sigma}{6e(\lambda)d}\right]^3 \tag{37}$$

where d is the diameter of the mother bubble and d_1 is the diameter of the smaller daughter bubble. When a bubble with diameter d (or volume v) breaks into a daughter bubble of size vf_v and a complement bubble of size $v(1 - f_v)$, the surface energy increase is

$$\Delta e_i(f_v, d) = [f_v^{2/3} + (1 - f_v)^{2/3} - 1]\pi d^2\sigma = c_f\pi d^2\sigma \tag{38}$$

To cause bubble breakup, the eddy energy $e(\lambda)$ should be larger than or equal to the increase of surface energy $\Delta e_i(f_v, d)$, that is

$$e(\lambda) \geq c_f\pi d^2\sigma \tag{39}$$

$$c_{f,\max} = \min\left[(2^{1/3} - 1), \frac{e(\lambda)}{\pi d^2\sigma}\right] \tag{40}$$

The maximum breakup fraction $f_{v,\max}$ is then determined from $c_{f,\max}$ by Eq. 38. Thus, when a bubble of size d is hit by an eddy of size λ and kinetic energy $e(\lambda)$, the possible breakup fraction is between $f_{v,\min}$ and $f_{v,\max}$. The probability of a bubble of size d breaking with breakup fraction f_v is considered to be the same, and is determined by

$$P_b(f_v|d, e(\lambda), \lambda) = \begin{cases} \dfrac{1}{f_{v,\max} - f_{v,\min}} & f_{v,\max} - f_{v,\min} \geq 0.01 \\ & f_{v,\min} < f_v < f_{v,\max} \\ 0 & \text{else} \end{cases} \tag{41}$$

To calculate $P_b(f_v \mid d, \lambda)$, the energy distribution of turbulent eddies is needed. The energy distribution of eddies of size λ is as follows

$$P_e[e(\lambda)] = \frac{1}{\bar{e}(\lambda)}\exp[-e(\lambda)/\bar{e}(\lambda)] \tag{42}$$

where $\bar{e}(\lambda)$ is the mean kinetic energy:

$$\bar{e}(\lambda) = \frac{\pi}{6}\lambda^3\rho_l\frac{\bar{u}_\lambda^2}{2} \tag{43}$$

The probability of a bubble of size d breaking with breakup fraction f_v when hit by a turbulent eddy of size λ is then calculated by

$$P_b(f_v|d, \lambda) = \int_0^\infty P_b[f_v|d, e(\lambda), \lambda]P_e[e(\lambda)]de(\lambda) \tag{44}$$

Substituting Eqs. 35 and 44 into Eq. 34, the breakup rate of a bubble of size d breaking with breakup fraction f_v is obtained as

$$b(f_v|d) = 0.923(1 - \alpha_d)n\varepsilon^{1/3}\int_{\lambda_{\min}}^{d_b} P_b(f_v|d, \lambda)(\lambda + d)^2\lambda^{-11/3}d\lambda \tag{45}$$

where the minimum eddy size in the inertial subrange $\lambda_{\min}$ is taken to be 31.4 times the Kolmogorov length scale (Tennekes and Lumley, 1973).

The total breakup rate can be calculated by

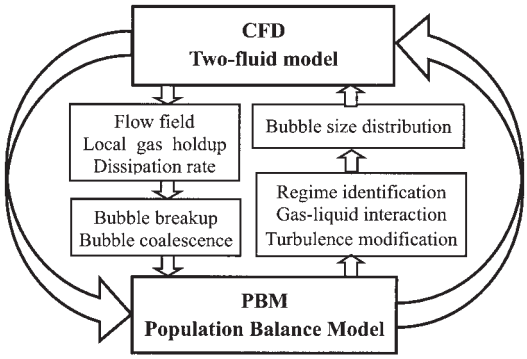

Figure 2. Coupled mode in the CFD-PBM coupled model.

$$b(d) = \int_0^{0.5} b(f_v|d)df_v \tag{46}$$

The daughter particle size distribution is as follows

$$\beta(f_v, d) = \frac{b(f_v|d)}{\int_0^{0.5} b(f_v|d)df_v} \tag{47}$$

Note that the calculation of the bubble breakup rate and the daughter bubble size distribution is time consuming because a triple integral is involved. Wang et al. (2004a) subsequently proposed an efficient numerical algorithm for the model.

Breakup Resulting from Instability. A bubble with size larger than a certain critical value will break up quickly because of the instability of the bubble surface. Following Carrica and Clausse (1993), the bubble breakup rate stemming from this mechanism was estimated by

$$b_2(d) = b^* \frac{(d - d_{c2})^m}{(d - d_{c2})^m + d_{c2}^m} \tag{48}$$

where d_{c2} is the critical bubble diameter. Carrica and Clausse (1993) suggested that the critical Weber number (We) takes a value of 100 for an air–water system, which corresponds to $d_{c2} = 27$ mm. b^* and m are model parameters, and were set to be 100 1/s and 6.0, respectively. Because detailed studies are not available for this bubble breakup process, the bubble was assumed to break into two equal daughter bubbles with the consideration that nonuniform breakup of a large bubble has already been included in the breakup model ascribed to turbulent mechanism.

CFD-PBM Coupled Model

Figure 2 shows the schematic of the coupled mode in the CFD-PBM coupled model: the gas holdup and kinetic energy dissipation rate calculated by CFD are used to solve the PBM, and the bubble size distribution is used to calculate the interphase forces and turbulence modification in the two-fluid model. Only one common velocity field is calculated for all bubble classes. The different slip velocities of bubbles within different groups are needed in the calculation of bubble coalescence caused by different rise velocities. Sha et al. (2004) described each bubble fraction by one Eulerian phase to get the velocity field for each bubble group. In fact, the slip velocity of bubbles within different groups can be directly calculated from the drag force formulation and balance between the drag and buoyancy forces on a bubble. This is also confirmed by comparing the bubble rise velocities given by Sha et al. (2004) with those calculated from the drag force formulation.

The equations governing the dynamics of two-phase flows have been much discussed in the literature. The main difficulty in the two-fluid model is the modeling of the phase-interaction terms including the interphase forces and the interphase turbulence. The time-averaged governing equations for gas–liquid flows in steady state are listed as follows, and details are introduced in our previous work (Wang et al., 2004b).

Basic two-fluid equations

Mass Conservation

- Gas phase

$$\nabla \cdot (\rho_g \alpha_g \mathbf{u}_g) = 0 \tag{49}$$

- Liquid phase

$$\nabla \cdot (\rho_l \alpha_l \mathbf{u}_l) = 0 \tag{50}$$

Momentum Conservation

- Gas phase

$$\nabla \cdot (\rho_g \alpha_g \mathbf{u}_g \mathbf{u}_g) = -\alpha_g \nabla P' + \nabla \cdot [\alpha_g \mu_{\text{eff},g} (\nabla \mathbf{u}_g + \nabla \mathbf{u}_g^T)] + \mathbf{F}_{g,l} + \rho_g \alpha_g \mathbf{g} \tag{51}$$

- Liquid phase

$$\nabla \cdot (\rho_l \alpha_l \mathbf{u}_l \mathbf{u}_l) = -\alpha_l \nabla P' + \nabla \cdot [\alpha_l \mu_{\text{eff},l} (\nabla \mathbf{u}_l + \nabla \mathbf{u}_l^T)] - \mathbf{F}_{g,l} + \rho_l \alpha_l \mathbf{g} \tag{52}$$

where P' is a modified pressure defined by

$$P' = P + \frac{2}{3} \mu_{\text{eff},l} \nabla \cdot \mathbf{u}_l + \frac{2}{3} \rho_l k_l \tag{53}$$

The effective viscosity of the gas phase is $\mu_{eff,g} = \mu_{lam,g} + \mu_{t,g}$. The effective viscosity of the liquid phase $\mu_{eff,l}$ is (Sato and Sekoguchi, 1975)

$$\mu_{\text{eff},l} = \mu_{lam,l} + \mu_{t,l} + \mu_{tb} \tag{54}$$

$$\mu_{tb} = C_{\mu b} \rho_l \alpha_g d_{bs} |u_g - u_l| \tag{55}$$

where $C_{\mu b}$ was set to be 0.6.

Interphase forces

Drag Force

$$\mathbf{F}_D = \sum_{i=1}^{M} k_{b,\text{large}} f_i \alpha_g \rho_l \frac{3C_{Di}}{4d_{bi}} (\mathbf{u}_g - \mathbf{u}_l)|\mathbf{u}_g - \mathbf{u}_l| \tag{56}$$

$$C_{Di} = \max\left[\frac{24}{\text{Re}_i}(1 + 0.15\,\text{Re}_i^{0.687}), \frac{8}{3}\frac{\text{Eo}}{\text{Eo} + 4}\right] \tag{57}$$

The coefficient $k_{b,\text{large}}$ in Eq. 56 accounts for the wake acceleration effect of large bubbles, and was correlated to the fraction of large bubbles and local gas holdup

$$k_{b,\text{large}} = \max(1.0, 50.0\alpha_g f_{b,\text{large}}) \tag{58}$$

where $f_{b,\text{large}}$ is the fraction of large bubbles.

Virtual Mass Force

$$F_{VM} = \alpha_g \rho_l C_{VM} \frac{D}{Dt}(u_g - u_l) \tag{59}$$

where D/Dt is the material derivative.

Transverse Lift Force. The transverse lift force is calculated based on the correlation proposed by Tomiyama et al. (1999)

$$F_L = -\sum_{i=1}^{M} f_i C_{Li} \alpha_g \rho_l (u_g - u_l)\nabla u_l \tag{60}$$

$$C_{Li} = \begin{cases} \min(0.288\tanh(0.121\,\text{Re}_i), f(\text{Eo}_i')) & \text{Eo}_i' < 4 \\ f(\text{Eo}_i') & 4 < \text{Eo}_i' < 10 \\ -0.29 & \text{Eo}_i' > 10 \end{cases} \tag{61}$$

$$f(\text{Eo}_i') = 0.00105\,\text{Eo}_i'^3 - 0.0159\,\text{Eo}_i'^2 - 0.0204\,\text{Eo}_i' + 0.474 \tag{62}$$

where Eo_i is the modified Eötvös number based on the maximum horizontal dimension of the bubble. The aspect ratio of the maximum vertical dimension to the maximum horizontal dimension of the spheroidal bubble was evaluated with Wellek's empirical correlation (Wellek et al., 1966).

Turbulent Dispersion Force

$$F_{TD} = -C_{TD}\rho_l k_l \nabla\alpha \tag{63}$$

Wall Lubrication Force

$$F_W = -\sum_{i=1}^{M} f_i C_{Wi} \alpha_g \frac{d_{bi}}{2}\left[\frac{1}{(R-r)^2} - \frac{1}{(R+r)^2}\right]\rho_l (u_g - u_l)^2 \tag{64}$$

In the above equations, C_{VM}, C_{TD}, and C_{Wi} were set to be 0.25, 0.7 and 0.1, respectively.

Turbulence equations

Turbulent Viscosity

$$\mu_{t,l} = C_\mu(\rho_l k_l^2/\varepsilon_l) \tag{65}$$

k and ε Equations

$$\nabla\cdot(\rho_l\alpha_l k_l \mathbf{u}_l) = \nabla\cdot\{\alpha_l[\mu_{lam,l} + (\mu_{t,l} + \mu_{tb})/\sigma_k]\nabla k_l\} + \alpha_l(G_{k,l} - \rho_l\varepsilon_l) \tag{66}$$

$$\nabla\cdot(\rho_l\alpha_l\varepsilon_l \mathbf{u}_l) = \nabla\cdot\{\alpha_l[\mu_{lam,l} + (\mu_{t,l} + \mu_{tb})/\sigma_\varepsilon]\nabla\varepsilon_l\} + \alpha_l\frac{\varepsilon_l}{k_l}(C_{\varepsilon 1}G_{k,l} - C_{\varepsilon 2}\rho_l\varepsilon_l) \tag{67}$$

$$G_{k,l} = \mu_{\text{eff},l}\nabla\mathbf{u}_l\cdot[\nabla\mathbf{u}_l + (\nabla\mathbf{u}_l)^T] - \frac{2}{3}\nabla\cdot\mathbf{u}_l(\mu_{\text{eff},l}\nabla\cdot\mathbf{u}_l + \rho_l k_l) \tag{68}$$

The two time constants model proposed by de Bertodano et al. (1994) was used to calculate the kinetic energy and its dissipation rate of the liquid phase, that is,

$$k_{l,t} = k_l + k_{l,g} \tag{69}$$

$$\varepsilon_{l,t} = \varepsilon_l + \varepsilon_{l,g} \tag{70}$$

where $k_{l,t}$ and $\varepsilon_{l,t}$ are the total kinetic energy and dissipation rate, respectively, k_l and ε_l are calculated by the standard k–ε model, $k_{l,g}$ and $\varepsilon_{l,g}$ are the additional kinetic energy and dissipation rate caused by bubbles, respectively, and can be estimated by

$$k_{l,g} = 0.25\alpha_g u_{\text{slip}}^2 \tag{71}$$

$$\varepsilon_{l,g} = \alpha_g g u_{\text{slip}} \tag{72}$$

The apparent turbulent viscosity of the gas phase is calculated by

$$\mu_{t,g} = \mu_{t,l}\rho_g/\rho_l \tag{73}$$

Modified population balance equation

The general form of the convection–diffusion equation of the two-fluid model is

$$\frac{\partial}{\partial t}(\rho\alpha\varphi)_i + \nabla\cdot(\rho\alpha\varphi\mathbf{u})_i = \nabla(\Gamma\nabla\varphi)_i + S_\varphi \tag{74}$$

To cast the population balance equation into the same form as the generic convection–diffusion equation for multiphase flow, some modification is needed, taking into consideration that the

bubble number density and the gas holdup has the following relationship:

$$\alpha_g f_i = N_i v_i \tag{75}$$

where f_i is the volume fraction of group i in the gas holdup, and v_i is the volume of a bubble with size d_i. Substituting Eq. 75 into Eq. 9 yields

$$\frac{\partial}{dt}(\alpha_g f_i) + \nabla \cdot (\alpha_g \mathbf{u}_h f_i) = \sum_{\substack{j,k \\ x_{i-1} \le (x_j + x_k) \le x_{i+1}}}^{j \ge k} \times \left(1 - \frac{1}{2}\delta_{j,k}\right)\eta_{i,jk} c_{j,k} \alpha_g f_j \alpha_g f_k v_i / v_j / v_k - \alpha_g f_i \sum_{k=1}^{M} c_{i,j} \alpha_g f_k / v_k + \sum_{k=i}^{M} n_{i,k} b_k \alpha_g f_k v_i / v_k - b_i \alpha_g f_i \tag{76}$$

Equations 49 to 73 and 76 form the CFD-PBM coupled model, with the complement bubble coalescence and breakup kernel functions expressed by Eqs. 11 to 48.

Numerical Details

The simulation domain is between the perforated plate and the top of the column. Uniform inlet boundaries were used for both the gas and liquid phases. The boundary conditions for the inlet are as follows:

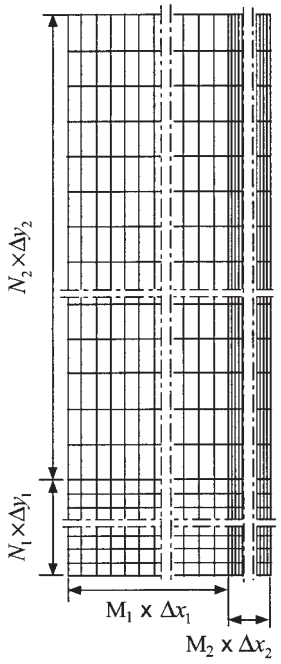

Figure 3. Grids used in the simulations.

Grid I: $M_1 = 10$, $\Delta x_1 = 0.0076$, $M_2 = 10$, $\Delta x_2 = 0.0019$, $N_1 = 10$, $\Delta y_1 = 0.03$, $N_2 = 20$, $\Delta y_2 = 0.105$; *Grid II*: $M_1 = 15$, $\Delta x_1 = 0.005$, $M_2 = 15$, $\Delta x_2 = 0.00133$, $N_1 = 15$, $\Delta y_1 = 0.02$, $N_2 = 30$, $\Delta y_2 = 0.07$.

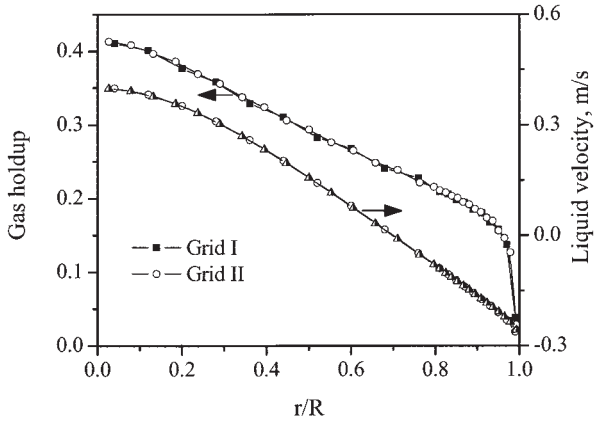

Figure 4. Influence of the grid on the simulations.

$$u_{g,in} = U_g / \bar{\alpha}_{g,in} \qquad u_{l,in} = U_{l,D} / (1 - \bar{\alpha}_{g,in})$$

$$k_{l,in} = 0.004 u_{l,in}^2 \qquad \varepsilon_{l,in} = C_\mu^{3/4} k_{in}^{3/2} / (0.07D)$$

$$\alpha_{g,in} = \bar{\alpha}_{g,in}$$

Fully developed flow conditions were used at the top and symmetrical conditions were applied at the center axis for all the variables. The wall function was used for the liquid phase and the nonslip condition for the gas phase.

CFX 4.4 (AEA Technology, Harwell, UK) was used to solve the CFD-PBM coupled model. In the CFX package, the transport equations for additional scalars are assumed to have the same form as the general scalar convective–diffusion equation, as shown in Eq. 74. The population balance equations were added to the CFX program by modifying the source term and diffusivity coefficients according to the proposed model through the user-defined routines. The gas phase was considered as incompressible. This is acceptable when the column height is <2.0 m.

Results and Discussion

Grid independence

Because of the axial symmetry, a two-dimensional grid for only half of the region was used in the numerical simulations. To attain grid-independent results, the influence of the grid on the simulation is studied. The grid used in this work is nonuniform, with finer mesh close to the inlet and the wall, as shown in Figure 3. The results for the radial profiles of the gas holdup and liquid velocity are shown in Figure 4. There is no perceptible difference between the results using *Grid I* and *Grid II*; therefore *Grid I* was used for all simulations in this work. It should be pointed out that this grid independence is valid only for 2-D steady-state simulations. The grid used here is not fine enough for 3-D transient simulations.

The bubble size was divided into M sections as follows

$$v_1 = 1.0 \times 10^{-10}\ \mathrm{m}^3$$

$$v_{i+1} = v_i r$$

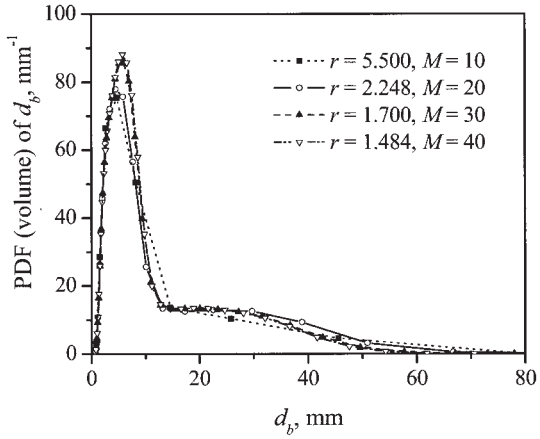

Figure 5. Influence of the number of bubble groups on the calculated bubble size distribution.

U_g = 0.12 m/s, α_g = 0.37, ε = 2.0 m^2/s^3.

$$x_i = 0.5(v_i + v_{i+1}) \qquad i = 1, 2, 3 \cdots M - 1$$

The bubble population between sizes v_i and v_{i+1} is represented by a pivot size x_i, as shown in Figure 1. The grid sensitivity was tested and the results are shown in Figure 5. The number of bubble groups M has no significant influence on the calculated bubble size distribution when M is >30. Therefore all the simulations in this work used the bubble size division with M = 30 and r = 1.7.

Different coalescence and breakup models

Figures 6a, 6b, 6c, and 6d compare the predicted bubble size distributions at the centerline in a bubble column in different flow regimes when different bubble coalescence and breakup models are used. The gas fraction and kinetic energy dissipation rate are from CFD simulations with the drag force calculated using Krishna's two-class bubble approach (Krishna et al., 1999). Four types of bubble breakup and coalescence models were compared: Prince's model (Prince and Blanch, 1990), Luo's model (Luo and Svendsen, 1996a,b), Lehr's model (Lehr et al., 2002), and the model of this work. Both the Prince and Luo models fail to predict the formation of large bubbles in the heterogeneous regime, and predict a tendency that bubbles become smaller with increasing superficial gas velocity, which is contrary to the experimental observation. Both models of Lehr et al. (2002) and of this work successfully predict the remarkably different bubble size distributions in different flow regimes and the formation of large bubbles in the heterogeneous regime. The results by these two models are quite similar at superficial gas velocities of 0.03 and 0.05 m/s. At the superficial gas velocity of 0.12 m/s, Lehr's model predicts a too distinct bimodal bubble size distribution with the two peaks at about 2.0 and 32 mm, respectively. The volume fractions of bubbles between 10 and 20 mm are almost zero, which seems unreasonable both from experimental observation and theoretical analysis.

Average gas holdup

When the flow is in different regimes, the average gas holdup shows different variations with the superficial gas velocity. The flow is in the homogeneous regime at low superficial gas velocities, where bubble interaction is relatively week and the average gas holdup increases almost linearly with the superficial gas velocity. With an increase in U_g, the bubble interaction becomes stronger and more large bubbles are formed as a result of bubble coalescence. When the flow enters the heterogeneous regime, the volume fraction of large bubbles increased substantially. Large bubbles have strong wake effects, and result in a reduction in the drag force and a slower increase in the gas holdup with the superficial gas velocity in the heterogeneous regime than in the homogeneous regime.

Figure 7 shows the simulation results with the CFD-PBM coupled model and with the CFD model that does not take into account the influences of the bubble size on the interphase forces. In the latter, the bubble size is set to be 7.0 mm for all cases. The results show that the CFD-PBM coupled model give reasonable results both in the homogeneous and heterogeneous regimes. However, the CFD model gives good agreement only for the average gas holdup in the homogeneous regime, and predicts an approximately linear increase in the gas holdup in all superficial gas velocity range, thus greatly overpredicting the gas holdup in the heterogeneous regime. In the CFD-PBM coupled model, both the influence of the bubble size on the drag force and the wake effect of large bubbles are considered, and thus the model is closer to the real situation. In the CFD-PBM coupled model, the deviation from the single bubble size drag model is taken into account because the formation of large bubbles is naturally included, as will be discussed below. Note that the CFD-PBM coupled model that does not take into account the wake effect of large bubbles predicts a gas

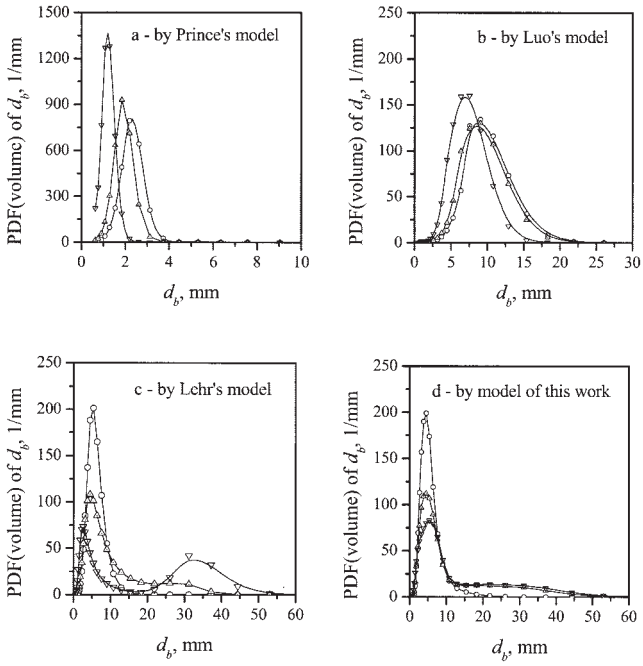

Figure 6. Bubble size distribution in the centerline of the bubble column predicted by different breakup and coalescence models.

Symbols: ○, U_g = 0.03 m/s, α_g = 0.109, ε = 0.30 m^2/s^3; △, U_g = 0.05 m/s, α_g = 0.21, ε = 0.62 m^2/s^3; ▽, U_g = 0.12 m/s, α_g = 0.37, ε = 2.0 m^2/s^3.

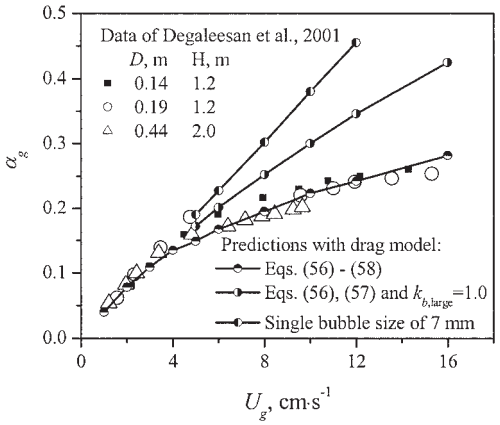

Figure 7. Comparison of measured and simulated average gas holdup.

Parameters of the simulated column: ID = 0.19 m, H = 2.4 m. The results are for a height of 2.0 m.

holdup lower than that of the single bubble size model, but still gives predictions that exceed the experimental values. Therefore, it is necessary to take into account the wake effect of large bubbles on accelerating rising bubbles at high superficial gas velocities.

Bubble size distribution

The bubble size distribution is determined by bubble coalescence and breakup. In a given system, bubble coalescence and breakup are primarily influenced by the local gas holdup and kinetic energy dissipation rate. Because of the nonuniform radial profiles of the gas holdup and dissipation rate, especially in the heterogeneous regime, the bubble size distribution varies with the radial position as well. Figure 8 shows the bubble size distribution at different radial positions and superficial gas velocities. At low superficial gas velocities, the bubble size distributions at different radial positions are quite similar. With an increase in the superficial gas velocity, the difference of the bubble size distributions at different radial positions becomes distinct, especially after the flow enters the heterogeneous regime. In the heterogeneous regime, the volume fraction of large bubbles in the central region increases significantly and the bubble size distribution has an obvious tail, indicating a transition of the gas-phase structure. Figure 8 also shows that in the wall region the variation of the bubble size distribution with the superficial gas velocity is not as remarkable as that in the central region, indicating that the bubbles in the central region play an important role in determining the gas-phase structure and the flow-regime transition.

Radial profiles of gas holdup and liquid velocity

For a further discussion of the gas-phase structure, bubbles are divided into small and large bubble groups based on a critical bubble size. This critical bubble size is 10 mm for the air–water system (Fu and Ishii, 2002). Figure 9 shows the radial profiles of the total gas holdup, gas holdup of small bubbles, and gas holdup of large bubbles. At low superficial gas velocities, the volume fraction of large bubbles is small and the flow is in the homogeneous regime. With an increase in the superficial gas velocity, the gas holdup of large bubbles substantially increases, which indicates a transition in the gas-phase structure and the flow transition from the homogeneous to the heterogeneous regime. Figure 9 also shows that at relatively high superficial gas velocities, the gas holdup of small bubbles has a much more uniform radial profile and increases more slowly than the gas holdup of large bubbles with increasing superficial gas velocity. The simulation results show that large bubbles are mainly present in the central region. This is in agreement with the observed phase structure in a bubble column reported by Chen et al. (1994), as shown in Figure 10. In the heterogeneous regime, the gas holdup presents a typical parabolic radial profile, which explains the stronger bubble coalescence and greater number of large bubbles in the central region.

Figures 11 and 12 show the radial profiles of the gas holdup and liquid velocity, respectively. In the homogeneous regime, the radial profile of the gas holdup is uniform, and the liquid circulation is relatively weak, whereas in the heterogeneous regime, the radial profile of the gas holdup is nonuniform and the liquid circulation is enhanced. It can be seen that the CFD-PBM model has good ability to predict the hydrodynamics in both the homogeneous and the heterogeneous regimes, and thus is applicable to much wider conditions than is the conventional CFD model.

Hydrodynamics of cocurrent upward flow

In bubble columns with $U_l = 0$, when the flow is in the homogeneous regime, the radial profile of the gas holdup is relatively uniform, but generally does not show a typical wall-peak. When the flow is in the heterogeneous regime, the gas holdup has a typical parabolic radial profile. For gas–liquid upward cocurrent flows, the gas holdup usually has a typically wall-peaking radial profile at high liquid velocity or low gas velocity (Ohnuki and Akimoto, 2000; Wang et al., 1987). Simulations were carried out with the CFD-PBM coupled model to study the hydrodynamics in such systems. Figure 13 is the comparison between the measured and predicted radial profiles of the gas holdup at the same superficial liquid velocity and different superficial gas velocities. The radial profile of the gas holdup is wall-peaking at a low superficial gas velocity and high liquid velocity, and is core-peaking at a high superficial gas velocity and low liquid velocity. This is mainly explained by the influence of the bubble size on the lateral forces, including the magnitude and direction (Wang et al., 2004b). The agreement is satisfactory for all the operating conditions. The results show that for the prediction of the complex hydrodynamic behaviors in a wide range of operating conditions, it is necessary to take into account the bubble size distribution and its influences on the lateral forces and turbulence. The CFD-PBM coupled model takes into account the influence of the bubble size distribution on the lateral forces based on the predicted bubble size distribution, and thus succeeds in properly predicting different radial profiles of the gas holdup in different conditions. The relatively larger departure between the measured and predicted gas holdup near the wall indicates that further improvements on formulation of the bubble lateral forces are needed.

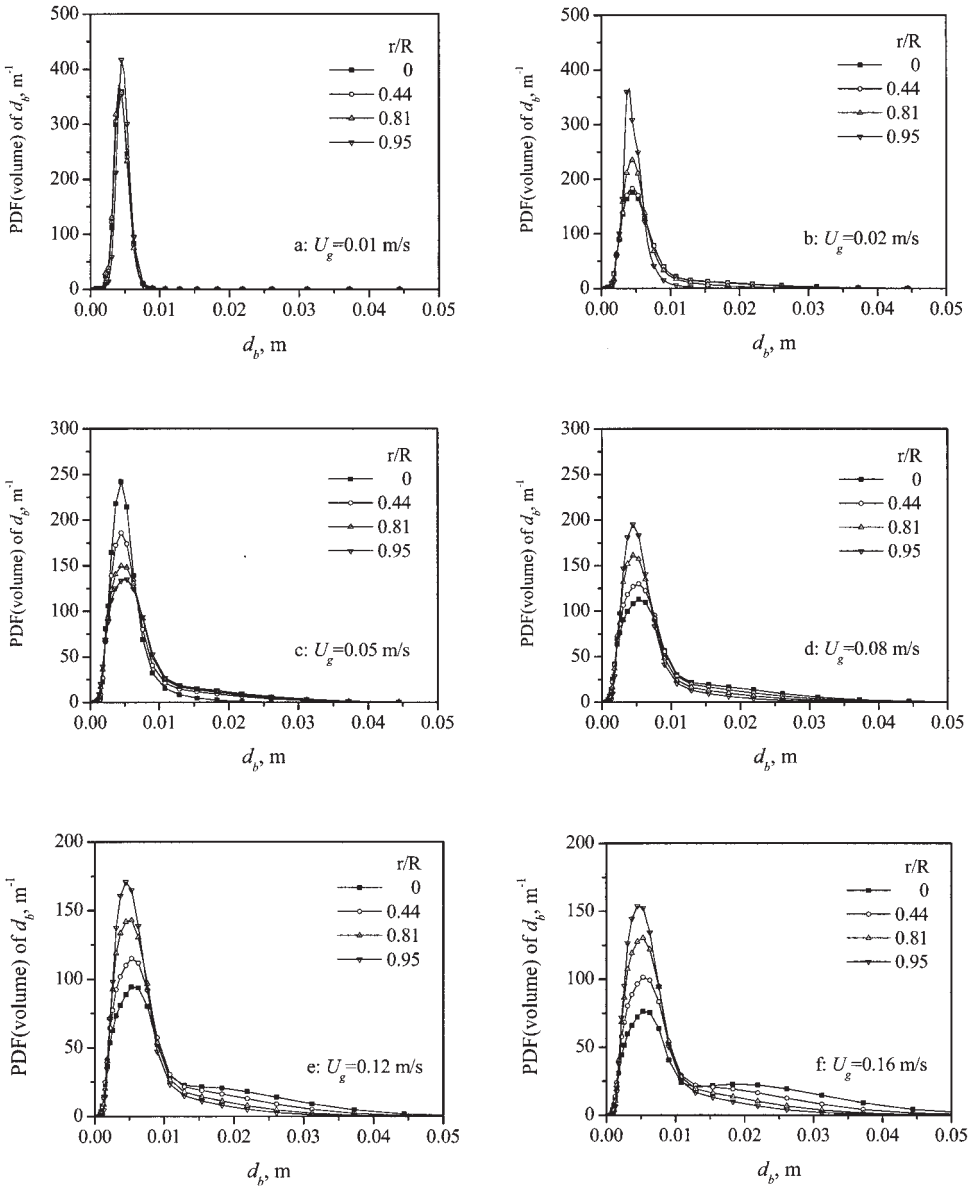

Figure 8. Bubble size distribution at different radial positions and different superficial gas velocities.

Parameters of the simulated column: $ID = 0.19$ m, $H = 2.4$ m. The results are for a height of 2.0 m.

Conclusions

A CFD-PBM coupled model was proposed that takes into account bubble breakup and coalescence behaviors and the influence of bubble size distribution on the phase interaction and turbulence. Four typical bubble breakup and coalescence models were compared. The results show that the bubble breakup and coalescence models are very important for properly predicting the bubble size distributions for both the homogeneous and the heterogeneous regimes. The influence of the lateral forces on the hydrodynamic behavior was considered and an algorithm was proposed for computing the interphase forces based on the bubble size distribution. By taking into account different mechanisms of bubble coalescence and breakup, the bubble size distribution was reasonably predicted for both the homogeneous and the heterogeneous regimes. Besides the drag force and virtual mass force, the lateral forces, including the transverse lift force, wall lubrication force, and turbulent dispersion force, were also considered. These interphase forces depend on the bubble size, and the bubble size distribution calculated by the PBM was used to quantify this dependency. Good agreement was obtained compared with the experimental gas holdup and liquid velocity, showing that the CFD-PBM coupled model has good ability to predict the hydrodynamic behavior in both the homogeneous and the heterogeneous regimes. The simulation results show that at low superficial gas velocities, the bubbles are small and have a narrow size distribution, and the gas holdup has a relatively uniform radial profile, which is the characteristic of the homogeneous regime; with an increase in the superficial gas velocity, bubble coalescence becomes stronger and greater numbers

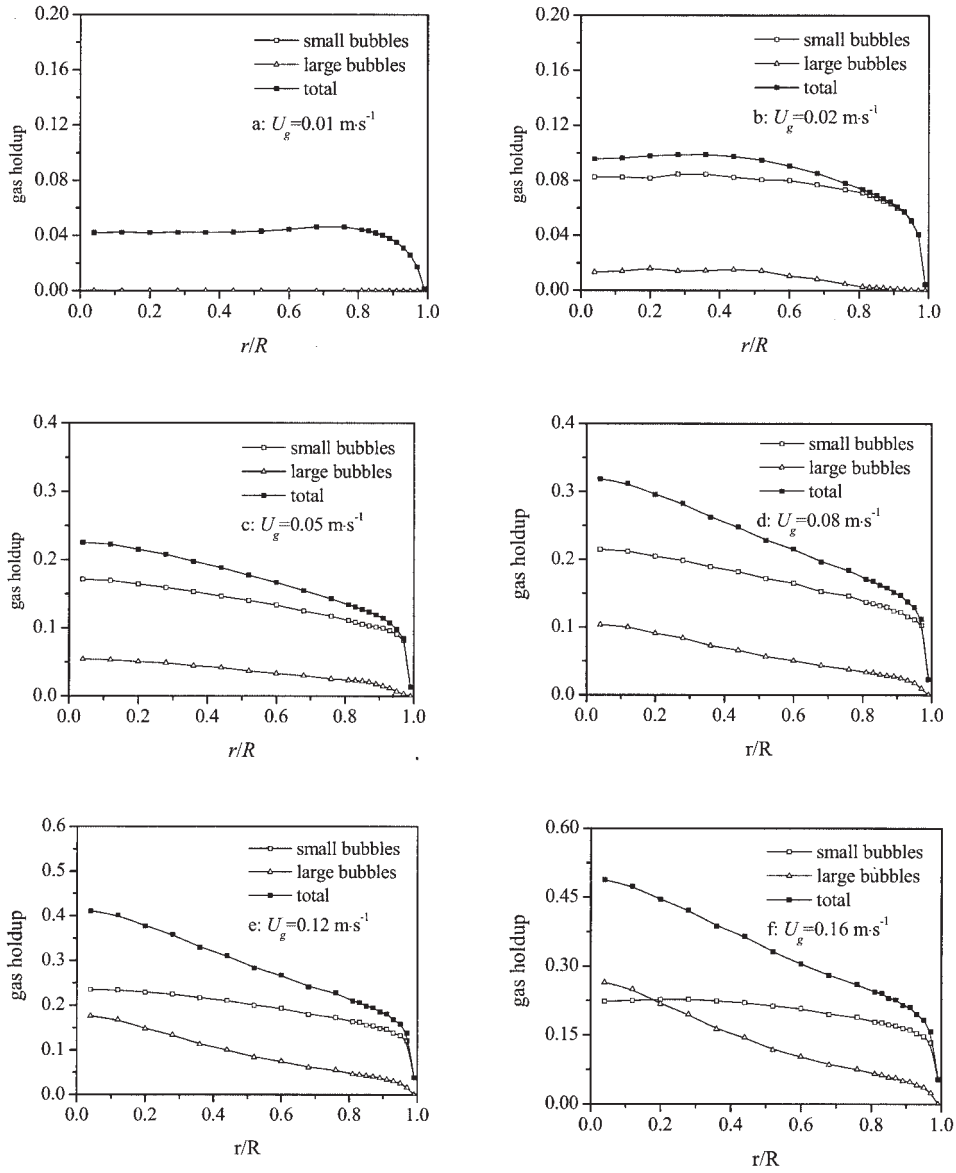

Figure 9. Radial profiles of the gas holdup for small bubbles, large bubbles, and total bubbles.

Parameters of the simulated column: ID = 0.19 m, H = 2.4 m. The results are for a height of 2.0 m.

of large bubbles are formed, leading to a more parabolic radial profile of the gas holdup and the transition from the homogeneous to the heterogeneous regime.

In summary, the CFD-PBM coupled model with the bubble breakup and coalescence models and the interphase force formulations in this work has the ability to predict the complex hydrodynamics in different flow regimes, and thus provides a unified description of both the homogeneous and the heterogeneous regimes. Further study will focus on improving the models for bubble coalescence and breakup, turbulence modification in high gas holdup, and interphase forces on bubble swarms.

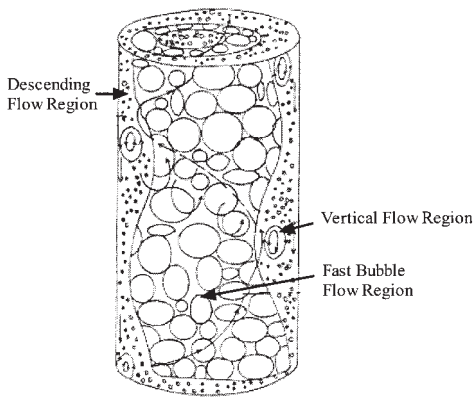

Figure 10 . Typical flow structure in a bubble column operated in the heterogeneous regime (Chen et al., 1994).

Acknowledgments

The authors gratefully acknowledge the financial supports by the Chinese National Science Foundation (No. 20276035).

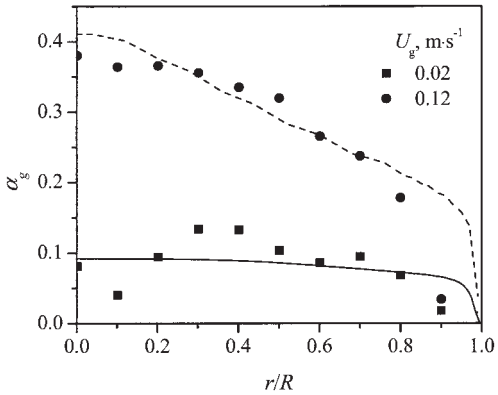

Figure 11. Radial profiles of the gas holdup in different flow regimes.

Symbols: Data of Sanyal et al. (1999): $ID = 0.19$ cm; $H = 1.0$ m. Lines: predictions by the CFD-PBM model.

Notation

$b(v)$ = bubble breakup rate, s^{-1}
$c(v_i, v_j)$, $c(d_i, d_j)$ = bubble coalescence kernel function, m^3 s^{-1}
c_f = parameter of increase of surface energy defined by Eq. 38
$c_{i,j}$ = abbreviation of $c(d_i, d_j)$, m^3 s^{-1}
C_L = lift force coefficient
C_{VM} = virtual mass force coefficient
C_W = wall lubrication force coefficient
d = diameter of the mother bubble, m
d_1 = diameter of the smaller daughter bubble, m
d_c = critical size of bubbles having wake effect for bubble coalescence, m
d_{c2} = critical size of bubbles with breakup resulting from instability, m
$e(\lambda)$ = kinetic energy of an eddy of size λ, J
$\bar{e}(\lambda)$ = mean kinetic energy of an eddy of size λ, J
Eo = Eötvös number, $g(\rho_l - \rho_g)d_b^2/\sigma$
Eo′ = modified Eötvös number, $g(\rho_l - \rho_g)d_{bH}^2/\sigma$
d_{bH} = maximum horizontal dimension of the bubble, m
F_L = transverse lift force, N m^{-3}
$\langle f_b,\text{large}\rangle$ = fraction of large bubbles
F_{TD} = turbulent dispersion force, N m^{-3}
f_v = breakup fraction defined by v_1/v
F_{VM} = virtual mass force, N m^{-3}
F_W = wall lubrication force, N m^{-3}
$G_{k,l}$ = turbulence production term in the liquid phase, J m^{-3} s^{-1}

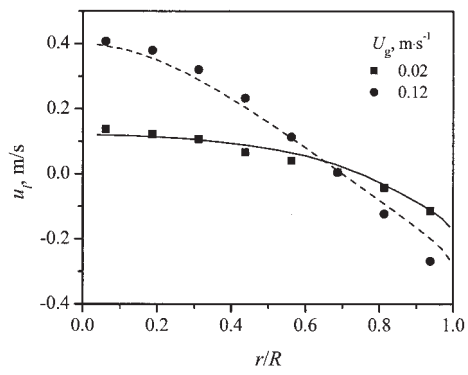

Figure 12. Radial profiles of the liquid velocity in different flow regimes.

Symbols are the same as in Figure 11.

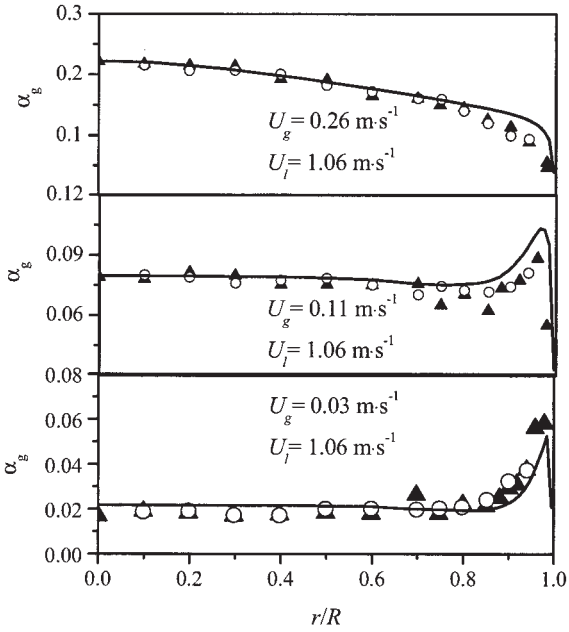

Figure 13. Radial profiles of the gas holdup in a gas–liquid cocurrent upward flow.

Note: Flow rate is based on the top section, and the predictions are for the fully developed section. Symbols: data from Ohnuki and Akimoto (2000): $ID = 0.2$ m, $H = 12$ m. Lines: predictions by the CFD-PBM model.

$h_{b,ij}$ = mean distance between bubbles of size d_i and d_j, m
k = kinetic energy, m^2 s^{-2}
k_b,large = model parameter accounting for bubble wake effect
L_w = length of the effective wake region, m
l_{bt} = bubble turbulent path, m
$l_{bt,ij}$ = mean relative turbulent path of bubbles of size d_i and d_j, m
M = number of bubble groups
n_λ = number density of eddy with size λ, m^{-3}
$n(v, t)$ = bubble number density function, m^{-6}
$N_i(t)$ = number of bubbles with volume between v_i and v_{i+1}, m^{-3}
$N_{wi,j}$ = number of bubbles of size d_j in the wake of a leading large bubble of size d_i
$P(d_i, dj)$ = bubble coalescence efficiency
$P_b[e(\lambda)]$ = energy-distribution density function for eddy of size λ, J^{-1}
$P_b(f_v \mid d, \lambda)$ = breakup probability for a bubble of size d breaking with breakup fraction f_v when hit by an eddy of size λ
$P_b[f_v \mid d, e(\lambda), \lambda]$ = breakup probability for a bubble of size d breaking with breakup fraction f_v when hit by an eddy of size λ and kinetic energy $e(\lambda)$
Re = bubble Reynolds number
$t_{i,j}$ = contact time when the bubble collision, s
$\mathbf{u}_b$ = bubble velocity, m s^{-1}
$\bar{u}_{ij}$ = mean relative turbulent velocity between bubbles of size d_i and d_j, m s^{-1}
$\bar{u}$ = mean turbulent velocity, m s^{-1}
v = volume of the mother bubble, m^3
v_1 = volume of the smaller daughter bubble, m^3
V_w = volume of the effective wake region, m^3
We_{ij} = Weber number, $\rho_l d_i \bar{u}_{ij}/\sigma$
x_i = pivot bubble size of the bubble interval (v_i, v_{i+1}), m^3

Greek letters

α = phase holdup
$\beta(v, v')$ = daughter bubble size distribution function
Γ_{ij} = model parameter
Δe_i = increase of surface energy during breakup, J
δ = model parameter
ε = dissipation rate of the kinetic energy, $m^2\ s^{-3}$
$\zeta_{i,k}$ = transfer coefficient between bubble groups arising from bubble breakup
$\eta_{i,jk}$ = transfer coefficient between bubble groups arising from bubble coalescence
Θ = model parameter
λ = eddy size, m
μ = viscosity, Pa·s
ξ_{ij} = relative size defined as d_i/d_j
ρ = density, kg m^{-3}
σ = surface tension, N m^{-1}
τ_e = lifetime of an eddy, s^{-1}
$\tau_{i,j}$ = time required for bubble coalescence, s
$\omega_1(v, x_i)$, $\omega 2(v, x_i)$ = bubble redistribution coefficient
$\varpi_\lambda(d)$ = collision frequency of eddies of size in (λ, $\lambda + d\lambda$) and bubbles of size d, s^{-1}
$\varpi(d_i, d_j)$ = specific collision frequency between bubbles of size d_i and d_j, $m^3\ s^{-1}$

Literature Cited

Bilicki, A., and J. Kestin, "Transition Criteria for Two-Phase Flow Patterns in Vertical Upward Flow," *Int. J. Multiphase Flow*, **13**, 283 (1987).

Carrica, P. M., and A. A. Clausse, "A Mathematical Description of the Critical Heat Flux as Nonlinear Dynamic Instability," *Instabilities in Multiphase Flow*. G. Gouesbet and A. Berlemont, eds., Plenum Press, New York (1993).

Chen, P., J. Sanyal, and M. P. Dudukoviæ, "Numerical Simulation of Bubble Columns Flows: Effect of Different Breakup and Coalescence Closures," *Chem. Eng. Sci.*, **60**, 1085 (2005).

Chen, R. C., J. Reese, and L. S. Fan, "Flow Structure in a Three-Dimensional Bubble Column and Three-Phase Fluidized Bed," *AIChE J.*, **40**, 1093 (1994).

Chesters, A. K., "Modelling of Coalescence Processes in Fluid-Liquid Dispersions: A Review of Current Understanding," *Trans. IChemE*, **69(A)**, 259 (1991).

Colella, D., D. Vinci, R. Bagatin, M. Masi, and E. A. Bakr, "A Study on Coalescence and Breakage Mechanisms in Three different Bubble Columns," *Chem. Eng. Sci.*, **54**, 4767 (1999).

de Bertodano, L. M., R. T. Lahey, and O. C. Jones, "Development of a k–ε Model for Bubbly Two-Phase Flow," *J. Fluids Eng.*, **116**, 128 (1994).

Degaleesan, S., M. Dudukovic, and Y. Pan, "Experimental Study of Gas-Induced Liquid Structures in Bubble Columns," *AIChE J.*, **47**, 1913 (2001).

Delnoij, E., F. A. Lammers, J. A. M. Kuipers, and W. P. M. Van Swaaij, "Dynamic Simulation of Dispersed Gas–liquid Two-Phase Flow Using a Discrete Bubble Model," *Chem. Eng. Sci.*, **52**, 429 (1997).

Drew, D. A., "Mathematical Modeling of Two-Phase Flow," *Ann. Rev. Fluid Mech.*, **15**, 261 (1983).

Fu, X. Y., and M. Ishii, "Two-Group Interfacial Area Transport in Vertical Air–Water Flow. I. Mechanistic Model," *Nucl. Eng. Des.*, **219**, 143 (2002).

Hibiki, T., and M. Ishii, "Two-Group Interfacial Area Transport Equations at Bubbly-to-Slug Transition," *Nucl. Eng. Des.*, **202**, 39 (2000).

Hills, J. H., "Radial Non-Uniformity of Velocity and Voidage in a Bubble Column," *Trans. IChemE*, **52**, 1 (1874).

Hua, J., and C. H. Wang, "Numerical Simulation of Bubble-Driven Liquid Flows," *Chem. Eng. Sci.*, **55**, 4159 (2000).

Hulburt, H., and S. Katz, "Some Problems in Particle Technology: A Statistical Mechanical Formulation," *Chem. Eng. Sci.*, **19**, 555 (1964).

Ishii, M., *Thermo-Fluid Dynamic Theory of Two-Phase Flow*, Eyrolles, Paris (1975).

Ishii, M., and N. Zuber, "Drag Coefficient and Relative Velocity in Bubbly, Droplet, or Particulate Flows," *AIChE J.*, **25**, 843 (1979).

Jakobsen, H. A., B. H. Sannes, S. Grevskott, and F. Svendsen, "Modeling of Vertical Bubble-Driven Flows," *Ind. Eng. Chem. Res.*, **36**, 4052 (1997).

Joshi, J. B., "Computational Flow Modeling and Design of Bubble Column Reactors," *Chem. Eng. Sci.*, **56**, 5893 (2001).

Kostoglou, M., and A. J. Karabelas, "On the Attainment of Steady State in Turbulent Pipe Flow of Dilute Dispersions," *Chem. Eng. Sci.*, **53**, 505 (1998).

Krishna, R., M. I. Urseanu, J. M. van Baten, and J. Ellenberger, "Influence of Scale on the Hydrodynamics of Bubble Columns Operating in the Churn-Turbulent: Experiments vs. Eulerian Simulations," *Chem. Eng. Sci.*, **54**, 4903 (1999).

Kronberger, T., A. Ortner, W. Zulehner, and H. J. Bart, "Numerical Simulation of Extraction Columns using a Drop Population Model," *Chem. Eng. Sci.*, **19**, S639 (1995).

Kumar, S., and D. Ramkrishna, "On the Solution of Population Balance Equations by Discretization—I. A Fixed Pivot Technique," *Chem. Eng. Sci.*, **51**, 1311 (1996).

Lahey, R. T., and D. A. Drew, "On the Development of Multidimensional Two-Fluid Models for Vapor/Liquid Two-Phase Flows," *Chem. Eng. Commun.*, **118**, 125 (1992).

Lee, C. H., L. E. Erickson, and L. A. Glasgow, "Bubble Break-up and Coalescence in Turbulent Gas–Liquid Dispersions," *Chem. Eng. Commun.*, **59**, 65 (1987).

Lehr, F., and D. Mewes, "A Transport Equation for the Interfacial Area Density Applied to Bubble Columns," *Chem. Eng. Sci.*, **56**, 1159 (2001).

Lehr, F., M. Millies, and D. Mewes, "Bubble-Size Distributions and Flow Fields in Bubble Columns," *AIChE J.*, **48**, 2426 (2002).

Levich, V. G., *Physicochemical Hydrodynamics*, Prentice-Hall, Englewood Cliffs, NJ (1962).

Liu, T. J., and S. G. Bankoff, "Structure of Air–Water Bubbly Flow in a Vertical Pipe—II. Void Fraction, Bubble Velocity and Bubble Size Distribution," *Int. J. Heat Mass Transfer*, **36**, 1061 (1993).

Lucas, D., E. Krepper, and H. M. Prasser, "Prediction of Radial Gas Profiles in Vertical Pipe Flow on the Basis of Bubble Size Distribution," *Int. J. Therm. Sci.*, **40**, 217 (2001).

Luo, H., and H. F. Svendsen, "Modeling and Simulation of Binary Approach by Energy Conservation Analysis," *Chem. Eng. Commun.*, **145**, 145 (1996a).

Luo, H., and H. F. Svendsen, "Theoretical Model for Drop and Bubble Breakup in Turbulent Dispersions," *AIChE J.*, **42**, 1225 (1996b).

Millies, M., and D. Mewes, "Interfacial Area Density in Bubble Flow," *Chem. Eng. Process.*, **38**, 307 (1999).

Ohnuki, A., and H. Akimoto, "Experimental Study on Transition of Flow Pattern and Phase Distribution in Upward Air–Water Two-Phase Flow along a Large Vertical Pipe," *Int. J. Multiphase Flow*, **26**, 367 (2000).

Olmos, E., C. Gentric, C. Vial, G. Wild, and N. Midoux, "Numerical Simulation of Multiphase Flow in Bubble Column Reactors. Influence of Bubble Coalescence and Breakup," *Chem. Eng. Sci.*, **56**, 6359 (2001).

Pan, Y., M. P. Dudukovic, and M. Chang. "Dynamic Simulation of Bubbly Flow in Bubble Columns," *Chem. Eng. Sci.*, **54**, 2481 (1999).

Pfleger, D., and S. Becker, "Modelling and Simulation of the Dynamic Flow Behaviour in a Bubble Column," *Chem. Eng. Sci.*, **56**, 1737 (2001).

Pohorecki, R., W. Moniuk, P. Bielski, and A. Zdrójkowski, "Modeling of the Coalescence-/Redispersion Processes in Bubble Columns," *Chem. Eng. Sci.*, **56**, 6157 (2001).

Prince, M. J., and H. W. Blanch, "Bubble Coalescence and Break-up in Air-Sparged Bubble Columns," *AIChE J.*, **36**, 1485 (1990).

Ramkrishna, D., *Population Balances*, Academic Press, San Diego, CA (2000).

Ramkrishna, D., and A. W. Mahoney, "Population Balance Modeling. Promise for the Future," *Chem. Eng. Sci.*, **57**, 595 (2002).

Sanyal, J., S. Vásquez, S. Roy, and M. P. Dudukovic, "Numerical Simulation of Gas–Liquid Dynamics in Cylindrical Bubble Column Reactors," *Chem. Eng. Sci.*, **54**, 5071 (1999).

Sato, Y., and K. Sekoguchi, "Liquid Velocity Distribution in Two-Phase Bubble Flow," *Int. J. Multiphase Flow*, **2**, 79 (1975).

Schlichting, H., *Boundary-Layer Theory*, McGraw-Hill, New York, NY (1979).

Sha, Z., A. Laari, I. and Turunen, "Implementation of Population Balance into Multiphase-Model in CFD Simulation for Bubble Column," Proc. of 16th Int. Congress of Chemical and Process Engineering, Prague, Czech Republic (2004).

Sokolichin, A., G. Eigenberger, A. Lapin, and A. Lübbert, "Dynamic Numerical Simulation of Gas–Liquid Two-Phase Flows: Euler–Euler versus Euler–Lagrange," *Chem. Eng. Sci.*, **52**, 611 (1997).

Svendsen, H. F., H. A. Jakobsen, and R. Torvik, "Local Flow Structure in

Internal Loop and Bubble Column Reactors," *Chem. Eng. Sci.*, **47**, 3297 (1992).
Tennekes, H., and J. L. Lumley, *A First Course in Turbulence*, The MIT Press, Cambridge, MA (1973).
Thakre, S. S., and J. B. Joshi, "CFD Simulation of Bubble Column Reactors: Importance of Drag Force Formulation," *Chem. Eng. Sci.*, **54**, 5055 (1999).
Tomiyama, A., H. Tamai, H. Shimomura, and S. Hosokawa, "Spatial Evolution of Developing Air–Water Bubble Flow in a Vertical Pipe," Proc. of 2nd Int. Symp. on Two-Phase Flow Modeling and Experimentation, Vol. II, Pisa, Italy, p. 1027 (1999).
Venneker, B. C. H., J. J. Derksen, and H. E. A. Van den Akker, "Population Balance Modeling of Aerated Stirred Vessels Based on CFD," *AIChE J.*, **48**, 673 (2002).
Wang, S. K., S. J. Lee, O. C. Jones Jr., and R. T. Lahey Jr., "3-D Turbulence Structure and Phase Distribution Measurements in Bubbly Two-Phase Flows," *Int. J. Multiphase Flow*, **13**, 327 (1987).
Wang, T. F., J. F. Wang, and Y. Jin, "A Novel Theoretical Breakup Kernel Function for Bubbles/Droplets in a Turbulent Flow," *Chem. Eng. Sci.*, **58**, 4629 (2003).
Wang, T. F., J. F. Wang, and Y. Jin, "An Efficient Numerical Algorithm for 'A Novel Theoretical Breakup Kernel Function of Bubble/Droplet in a Turbulent Flow'," *Chem. Eng. Sci.*, **59**, 2593 (2004a).
Wang, T. F., J. F. Wang, and Y. Jin, "Experimental Study and CFD Simulation of Hydrodynamic Behaviors in an External Loop Airlift Slurry Reactor," *Can. J. Chem. Eng.*, **82**, 1183 (2004b).
Wang, T. F., J. F. Wang, and Y. Jin, "The Population Balance Model for Gas–Liquid Flows—Influence of Bubble Coalescence and Breakup Models," *Ind. Eng. Chem. Res.*, in press.
Wellek, R. M., A. K. Agrawal, and A. H. P. Skelland, "Shapes of Liquid Drops Moving in Liquid Media," *AIChE J.*, **12**, 854 (1966).

Manuscript received Oct. 23, 2004, and revision received May 24, 2005.